Title
Two Faces of Mitral Stenosis: Uncovering Structural and Hemodynamic Signatures of Rheumatic and Mitral Annular Calcification—Induced Disease

Journal
Journal of the American Heart Association, 15(3)

ISSN
2047-9980

Authors
Hashemi, Mohammad S
Abdelmaseeh, Peter
Nehvi, Atif
et al.

Publication Date
2026-02-03

DOI
10.1161/jaha.125.045018

Journal of the American Heart Association

ORIGINAL RESEARCH

Two Faces of Mitral Stenosis: Uncovering Structural and Hemodynamic Signatures of Rheumatic and Mitral Annular Calcification–Induced Disease

Mohammad S. Hashemi, PhD; Peter Abdelmaseeh, MD; Atif Nehvi, MD; Gregg S. Pressman, MD; Arash Kheradvar, MD, PhD

BACKGROUND: Mitral annular calcification (MAC) is common and associated with increased cardiovascular risk and, when severe, mitral stenosis (MS). MAC-related MS differs anatomically and hemodynamically from rheumatic MS (RMS), challenging standard diagnostic methods. This study compares structural and flow characteristics, including kinetic energy losses, across MAC-related MS, RMS, and normal mitral valves, and evaluates the applicability of conventional diagnostic metrics in MAC.

METHODS: Three-dimensional transesophageal echocardiographic data sets from 70 patients (22 normal mitral valves, 26 RMS valves, 22 MAC valves) were used to obtain linear, area, and volumetric measurements for valve comparison. Representative valves from each group were converted into 3-dimensional silicone models for in vitro testing in a heart flow simulator. Transmitral flow was assessed with particle image velocimetry, flow energetics were quantified, and coefficients of contraction were derived from geometric and effective orifice areas.

RESULTS: Compared with RMS, MAC-related MS had smaller anteroposterior dimensions, reduced valve volume, and lower coefficients of contraction. MAC demonstrated the highest transmitral velocities and energy dissipation in vitro. Unlike the normal model, neither MAC nor RMS produced a consistent transmitral vortex ring. Despite having a larger geometric orifice, MAC MS produced a greater pressure drop than RMS, likely due to increased flow disruption and lower coefficients of contraction.

CONCLUSIONS: MAC-related MS represents a unique pathophysiological entity, characterized by distinct structural and hemodynamic features. These findings underscore the necessity for disease-specific diagnostic frameworks and multimodality imaging strategies to inform clinical decision making and guide emerging therapeutic approaches.

Key Words: 3-dimensional echocardiography ■ mitral annular calcification ■ particle image velocimetry ■ rheumatic mitral stenosis

Mitral annular calcification (MAC) is a common finding when imaging the heart. Population studies have estimated its prevalence at 8% to 15%, with increases noted in older age groups and patients with multiple cardiovascular risk factors.[1] MAC is also prevalent in individuals with chronic kidney disease[2] and those who have received radiation to the chest.[3] It is a marker of risk for adverse cardiovascular events, especially stroke,[4] and noncardiovascular events, including dementia and renal failure. Its presence is associated with increases in both cardiovascular and noncardiovascular death.[5]

When severe, MAC can cause valve dysfunction including both regurgitation and stenosis.[6] However,

Correspondence to: Arash Kheradvar, MD, PhD, FAHA, FASE, Professor of Radiological Sciences, Biomedical Engineering and Medicine, University of California, Irvine, 2420 Engineering Hall, Irvine, CA 92697-2730. Email: arashkh@uci.edu and Gregg S. Pressman, MD, FACC, Division of Cardiology, Jefferson Einstein Medical Center, Thomas Jefferson University, Philadelphia, PA. Email: gregg.pressman@jefferson.edu

This manuscript was sent to Amgad Mentias, MD, Associate Editor, for review by expert referees, editorial decision, and final disposition.

Supplemental Material is available at https://www.ahajournals.org/doi/suppl/10.1161/JAHA.125.045018

For Sources of Funding and Disclosures, see page 14.

JAHA is available at: www.ahajournals.org/journal/jaha

CLINICAL PERSPECTIVE

What Is New?

- Mitral annular calcification–related mitral stenosis is pathophysiologically distinct from rheumatic mitral stenosis, characterized by reduced valve volume, altered leaflet motion, disproportionately high transvalvular gradients, and unique flow dynamics despite relatively larger geometric orifice areas.
- Findings may inform the design of future transcatheter, and surgical therapies specifically tailored for mitral annular calcification–related stenosis.

What Are the Clinical Implications?

- Clinicians should be cautious when applying rheumatic-based diagnostic thresholds to mitral annular calcification–related mitral stenosis and recognition of mitral annular calcification–related stenosis as a distinct entity underscores the urgent need for disease-specific diagnostic criteria and treatment guidelines.

Nonstandard Abbreviations and Acronyms

CoC	coefficient of contraction
KE	kinetic energy
MAC	mitral annular calcification
MS	mitral stenosis
NMV	normal mitral valve
PIV	particle image velocimetry
RMS	rheumatic mitral stenosis
TEE	transesophageal echocardiography

MAC-related mitral stenosis (MS) differs substantially from that due to rheumatic disease, the classic cause of mitral stenosis. In particular, the 3-dimensional geometry of the 2 types of MS varies, but this variation has not been extensively studied. While rheumatic disease can feature some annular calcification, MS generally occurs due to commissural fusion and reduction in orifice area at the leaflet tips. By contrast, MS due to MAC typically features open commissures and bulky annular calcifications that extend onto the leaflets, restricting their mobility and displacing their hinge points apically.[7] In its most severe form – MAC produces a calcium "tunnel" within the annulus/leaflet complex.[8]

There are also important differences in the pathophysiology of MAC MS as compared with rheumatic MS (RMS) starting with the transvalvular pressure gradient. Doppler echocardiography has long been used in the clinic to measure this gradient in RMS.[9] Physicians have naturally applied the same approach to cases of MAC MS, but its Doppler velocity profile differs from that of RMS, and validation studies are lacking. Estimates of transmitral gradient based on the simplified Bernoulli equation can yield inaccurate results in MAC as the unsteady term of the general Bernoulli equation, representing time-dependent flow changes, is neglected.[10,11] Abnormal atrial and ventricular compliance, commonly present in patients with MAC, can also alter the Doppler velocity profile.[12] Thus, the same standard assessment of RMS cannot be applied to patients with MAC MS. From a clinical perspective, accurately determining the contribution of valvular dysfunction to symptoms of dyspnea and effort intolerance, which are common in these patients, can be challenging.

This investigation was conducted in 2 phases. The first phase involved systematic study of MAC valve geometry via 3-dimensional transesophageal echocardiography with comparisons made to RMS and normal mitral valve (NMV). The second phase of our research sought to better understand the changes in blood flow dynamics of the 2 valve pathologies. This involved 3-dimensional printing to create patient-specific silicone models of a healthy mitral valve, a rheumatic valve, and a MAC valve, which were then evaluated and compared in a heart flow simulator. This approach allowed us to isolate the effects of valve geometry variation while eliminating the influence of chamber compliance and flow rates.

METHODS

The echocardiographic data acquired and analyzed during this study, as well as the in vitro experimental data, are available from the corresponding authors upon reasonable request.

Study Design and Participants

We retrospectively analyzed previously – collected 3-dimensional echocardiographic data sets from 22 patients with NMV, 26 patients with rheumatic heart disease, and 22 patients with severe MAC (Table 1). All subjects had transesophageal echocardiography (TEE) performed for clinical indications. The collection and analysis of these data was approved by the Institutional

Table 1. Age and Sex by Valve Type

	Age, y, median (IQR)	Sex, female, %
NMV (n=22)	66 (58–77)	57
RMS (n=26)	70 (63–78)	43
MAC (n=22)	57 (44–67)	74

IQR indicates interquartile range; MAC, mitral annular calcification; NMV, normal mitral valve; and RMS, rheumatic mitral stenosis.

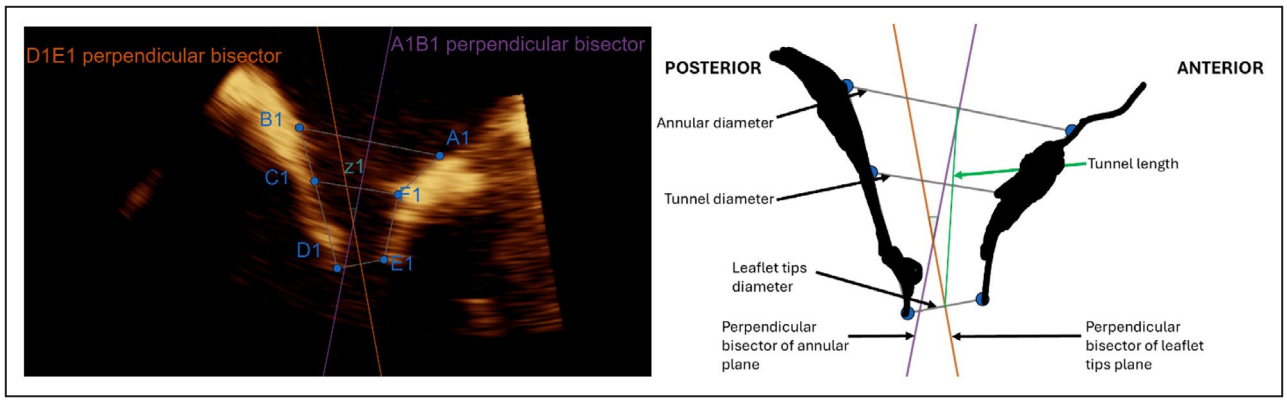

Figure 1. Anteroposterior echocardiographic view.
On the left is a 2-dimensional cross-sectional view, derived from a 3-dimensional data set, along the anteroposterior axis of a MAC valve. The slightly enlarged illustration on the right highlights key anatomic features and angle measurements. The anteroposterior diameters are measured at the annular plane (A1B1), the narrowest part of the mitral tunnel (C1F1), and the tip of the leaflets (D1E1). Distances are also given from the annular plane to the narrowest part of the tunnel (A1F1 and B1C1) and from the narrowest part to the leaflet tips (C1D1 and F1E1). Several angles (eg, z1) are defined to describe the orientation between these anatomic features, including whether the angle is clockwise (anterior) or counterclockwise (posterior). MAC indicates mitral annular calcification.

Review Board of Thomas Jefferson University. More specifically, the 3-dimensional data sets used in this study were collected under an Institutional Review Board–approved protocol with a waiver of informed consent, as the images were analyzed retrospectively after patient discharge.

Echocardiographic Measurements

TEE data sets were obtained using a Philips EPIQ-7 system equipped with an X7-2t or X8-2t probe. We started from the midesophageal 4-chamber view, optimizing the layout of the mitral valve, such that it was as nearly perpendicular to the ultrasound beam as possible. We then used the "3D Zoom" mode to focus on the valve leaflets and annulus, ensuring a minimum frame rate of 12 volumes/second. Care was taken to include the entire mitral annulus and the full length of the leaflets. The resultant 3-dimensional data sets were then analyzed using Philips QLAB (Philips Medical Systems, Andover, MA). Detailed measurements of annular and leaflet morphology were made (see Figures 1 and 2), along with measurements of the volume within the annulus/leaflet complex. The angles indicating which way the orifice points as compared with the annular plane (anterior/posterior, medial/lateral) were also measured (see Figures 1 and 2). Finally, we measured tunnel length (distance from the annular plane to the leaflet tips) and mitral valve volume from the annulus to the leaflet tips (in 57 subjects).

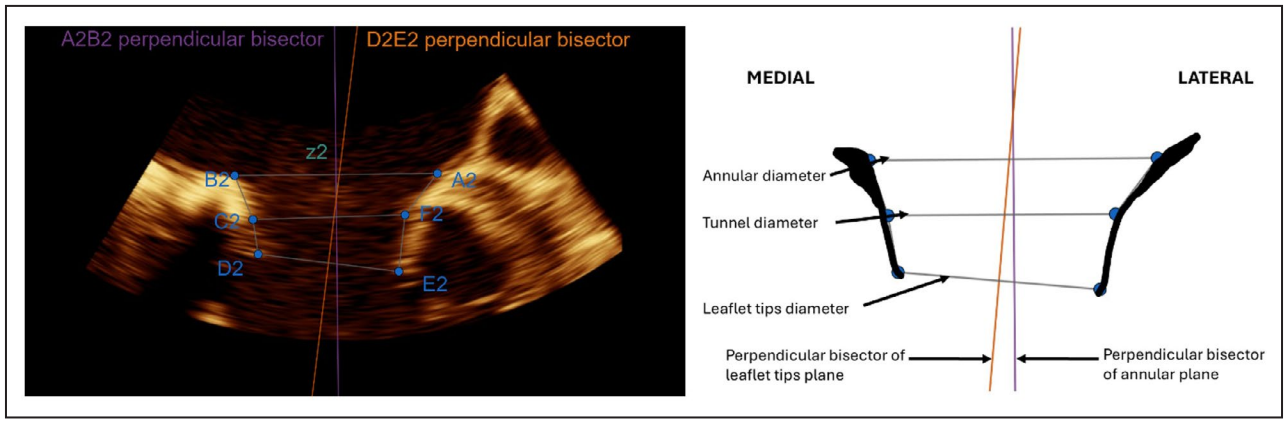

Figure 2. Intercommissural echocardiographic view.
On the left is a 2-dimensional cross-sectional plane, derived from a 3-dimensional data set, along the intercommissural axis of a MAC valve. The slightly enlarged sketch on the right highlights the key anatomic landmarks and angle measurements. The intercommissural diameters are measured at the annular plane (A2B2), the narrowest part of the mitral tunnel (C2F2), and the tip of the leaflets (D2E2). Distances are also shown from the annular plane to the narrowest part of the tunnel (A2F2 and B2C2) and from the narrowest part to the leaflet tips (C2D2 and F1E1). Various angles (eg, z2) are defined to describe the orientation between these features, noting whether the angle is clockwise (lateral) or counterclockwise (medial). MAC indicates mitral annular calcification.

Statistical Analysis

Categorical variables are presented as frequencies and percentages, while continuous variables are reported as medians with interquartile ranges. Comparisons of continuous variables were performed using either Student's *t* test or the Wilcoxon rank-sum test, as appropriate. A *P* value of <0.05 was considered statistically significant, except in cases involving multiple comparisons (eg, across the 3 valve groups), where the Bonferroni correction was applied. To quantify the impact of our results, we also present the power and effect sizes (Cohen's d) for the mean comparisons, assuming an α of 0.05, and 1-tailed hypotheses.

Three-Dimensional Silicone Models of Patient-Specific Mitral Valves

We chose 3 representative TEE data sets that were used to create silicone models of an NMV, RMS, and MAC valve. The orifice area of the RMS subject was 0.9 cm^2; for the MAC subject, it was 1.40 cm^2.

Three-dimensional TEE images were reviewed using Philips QLAB. We manually determined the echocardiographic frame where the mitral leaflets first contacted each other. This frame represented end-diastole. Data were then converted from standard 3-dimensional Digital Imaging and Communications in Medicine (DICOM) to Cartesian format once more using QLAB. Next, the Cartesian data set was converted to a specific format for 3-dimensional segmentation using ITK-SNAP version 3.8.0. The volume enclosed by the mitral valve and annulus was segmented thereby allowing for a "negative" 3-dimensional scaffold on which annulus and leaflets could be created from silicone. The scaffold was printed using polylactic acid on an Ender 3 printer (Creality Inc., Shenzhen, Guangdong, China). The mitral valve annulus and leaflets were created by painting 3 even coats of Smooth-on Ecoflex 00–20 (Smooth-On, Macungie, PA) on the 3-dimensionally printed mitral valve scaffold in our laboratory at Jefferson Einstein Medical Center. Afterward, application molds were placed into a 40 °C incubator for 2 hours to dry completely. In the case of the MAC valve, the calcium deposits were separately segmented and 3-dimensionally printed, again using polylactic acid. This was placed on the ventricular surface of the silicone valve print, and another thin layer of silicone was painted over it, thus incorporating the calcium phantom into the valve print. Figure 3 displays the resulting 3-dimensionally printed valve models. These models were then placed in the heart flow simulator at Kheradvar laboratory (KLAB) to allow evaluation of transmitral flow velocity profiles and energetics for each valve type. The valves were also segmented in midsystole to further highlight the differences in valve geometries (Videos S1 through S3).

Heart Flow Simulator for In Vitro Experimentation

A heart pulsed flow simulator at the University of California Irvine's KLAB, as described in our previous studies,[10,11] was used for in vitro experimental studies. The heart flow simulator is modular, enabling the use of a scaled-up, transparent left ventricular (LV) model made from thin silicone. This model is designed to accommodate proportionally scaled-up, 3-dimensionally printed valves that correspond with the dimensions of the patients' valves as determined from echocardiographic scans. The LV sac is suspended over a Plexiglas atrium, free-floating inside a rigid water-filled container (Figure 4). The Plexiglas atrium is designed to accommodate the 3-dimensionally printed valves. The LV sac contracts and expand due to a pulsatile pump (SuperPump system, VSI, SPS3891; ViVitro Systems Inc., Victoria, BC, Canada) simulating a normal physiological cardiac cycle.[10,12] The pump operates on the basis of a VSI Wave Generator (VG2001, ViVitro Systems Inc.), and we chose the waveform of frequency diverse array 70 beats/min for the experiments.[13] The maximum cardiac output set in our experiments was nominally 3.5 L/min due to the equipment limitation with a significantly upscaled LV model. The schematic configuration and images of the experimental setup are shown in Figure 4. A bioprosthetic valve (Biocor Valve Porcine Aortic, 26 mm; St. Jude Medical, Inc., Minneapolis, MN) was used as the aortic valve, while three 3-dimensionally printed valves were used at the mitral position, representing NMV, RMS, and MAC.

The LV chamber was illuminated with a laser sheet from a neodymium-doped yttrium lithium fluoride laser (Evolution 30; Coherent Corp., Saxonburg, PA) and images were captured at 1 kHz by a high-speed camera (Model Y3; Integrated Design Tools, Inc., Pasadena, CA). A pulse generator (565 Series Pulse Generator; Berkeley Nucleonics Corporation, San Rafael, CA) was used to synchronize the laser and high-speed camera.

Mapping Transmitral Flow

Two-dimensional particle image velocimetry (PIV) was used to map velocities from particle-seeded images over at least 2 heart cycles. For preprocessing, we applied contrast-limited adaptive histogram equalization. The main optical flow estimation was performed using fast Fourier transform window deformation, while SD and median filters were used for postprocessing the estimated velocity vectors from the acquired frame pairs. These methods were performed in the PIVlab 3.00 application, originally introduced by Stamhuis and Thielicke[14] in MATLAB software (MathWorks, Inc., Natick, MA) to calculate the flow fields. The numerical results were then processed in MATLAB and Excel (Microsoft Corp, Redmond, WA). Figure 5 illustrates a

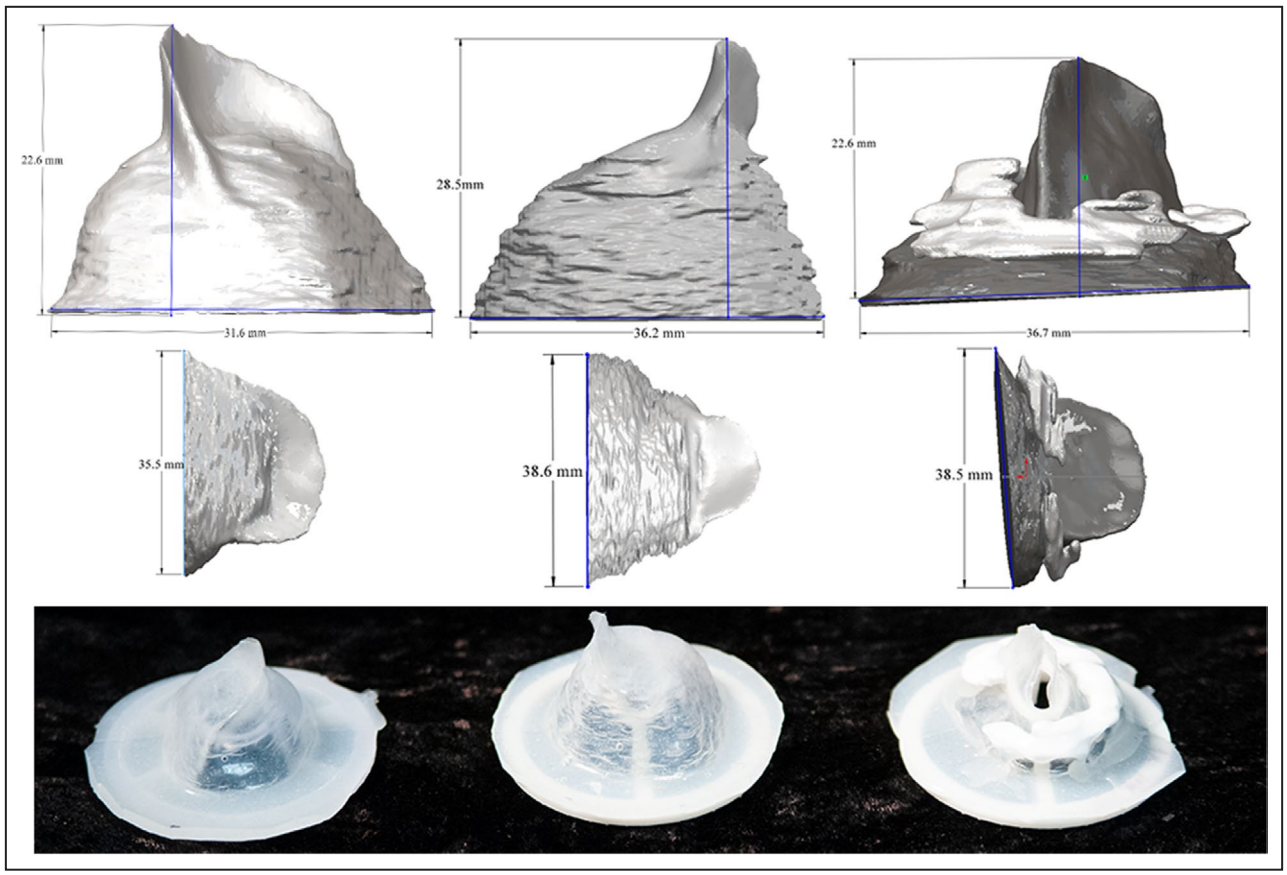

Figure 3. Three-dimensionally printed valve models for in vitro comparison of mitral valve conditions.
Left, NMV; middle, RMS; right, MAC. The top 2 rows display schematic figures of the mitral valve apparatus at leaflet closure, obtained via 3-dimensional echocardiography and scaled up for manufacturing. The bottom row shows photos of the models with backflow prevention features. The valves were created by coating 3-dimensionally printed plastic molds with silicone, with the MAC model additionally incorporating a 3-dimensionally printed calcification layer. Of note, the leaflet tips in the pictured models were intentionally lengthened to improve coaptation in the heart flow simulator (and minimize regurgitation); actual distances from the annulus center to the leaflet tips were 17 (NMV), 20 (RMS), and 14 mm (MAC). MAC indicates mitral annular calcification; NMV, normal mitral valve; and RMS, rheumatic mitral stenosis.

sample of 2-dimensional instantaneous LV flow fields obtained from PIV processing.

Since image acquisition in each experiment began at different phases of the cardiac cycle, synchronization was performed post hoc. To achieve this, the start of each signal (time=0) was aligned with the image pair that exhibited 0 or minimal mitral valve jet velocity, as determined by PIV analysis. Based on the frames and their corresponding videos, these time points align with the onset of the diastolic filling phase in each data set.

The main fluid dynamics quantities considered for comparison were the transmitral jet velocity and flow energetics, and more specifically the presence or absence of a consistent transmitral vortex ring. We compared transmitral flow velocity profiles for NMV, RMS, and MAC during a representative cardiac cycle in vitro. The velocity profiles downstream of the mitral valve were calculated by averaging the velocity magnitudes within a rectangular region of interest parallel to the mitral valve annulus. The region of interest width was set equal to the mitral valve diameter, while its length extended from one third to one half of the LV length measured from the mitral valve annulus plane, resulting in a total length equivalent to one sixth of the LV length. The velocity measured in the region of interest during diastole corresponds to the transmitral jet velocity, while the velocity measured during systole represents the jet approaching the mitral valve. To detect presence of transmitral vortex ring, we visualized the streamlines near the mitral valves and their changes throughout the captured cardiac cycles.

Coefficient of Contraction

The coefficient of contraction (CoC) for the mitral valve, representing the ratio of effective orifice area to geometric orifice area, is a critical parameter in assessing mitral valve function. In clinical practice, particularly when applying the Gorlin formula to calculate mitral valve area, an empirical coefficient of 0.85 is commonly

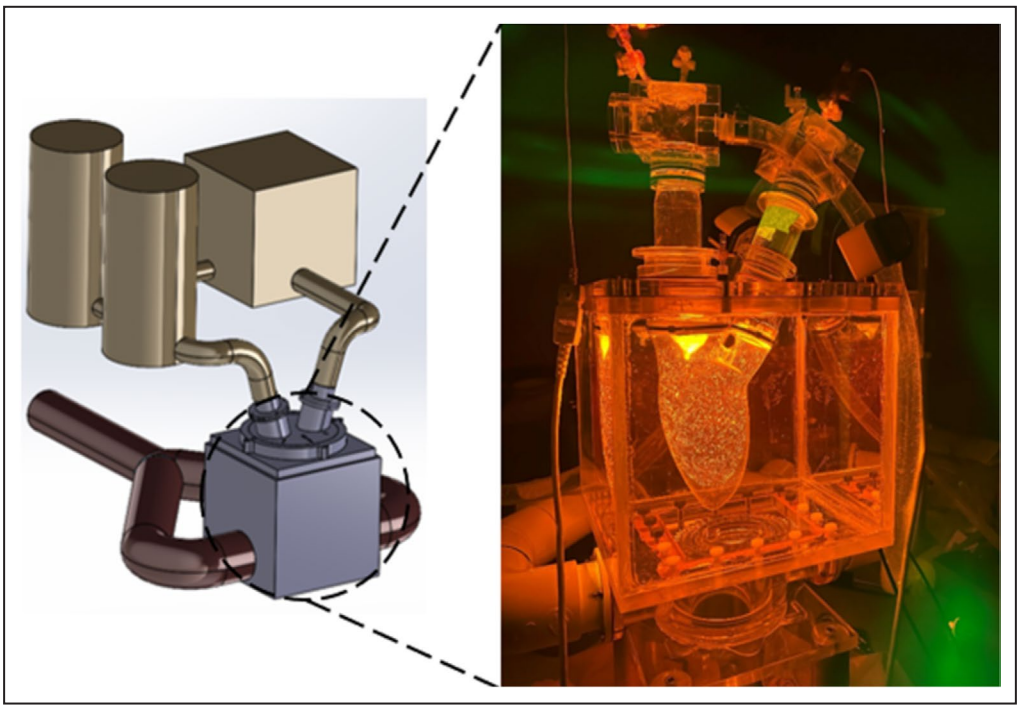

Figure 4. The KLAB heart flow simulator used for in vitro experimentation.
A photo showing a 2-dimensional frame capture from image sequences for PIV analysis. Taken with a smartphone camera through safety goggles, the green laser sheet appears orange. The mitral valve is placed on the left side of the left ventricular sac (right). A schematic diagram of the KLAB heart flow simulator setup is shown (left), which is adapted from Falahatpisheh and Kheradvar[10] . KLAB indicates Kheradvar laboratory; and PIV, particle image velocimetry.

used. This value was proposed by Cohen and Gorlin to better align calculated valve areas with those observed during surgery or autopsy.[15–17]

It is important to note that the CoC can vary on the basis of the 3-dimensional geometry of the mitral valve. For instance, Gilon et al[18] found that patients with doming mitral valves had higher CoCs compared with those with flat valves, resulting in higher pressure drops for those with flat valves, given the same geometric or anatomic orifice area. This variation underscores the influence of valve morphology on hemodynamic assessments. Three-dimensional echocardiography, as we used here, offers detailed insights into valve geometry, aiding in more precise calculations. We quantified the geometric orifice areas from the 3-dimensional data sets using a standard approach. Orthogonal views along the antero-posterior and intercommissural axes were generated, and a custom cut plane was placed at the level of the leaflet tips. Geometric orifice areas were measured on this plane. Effective orifice areas were then estimated by combining peak mitral jet velocities obtained from PIV analyses in the in vitro experiments with real-time flow rates measured using flowmeter devices:

$$\text{Effective orifice area} = \text{Highest measured flow rate} / \text{Highest mitral jet velocity} \quad (1)$$

Consequently, the CoC was calculated as:

$$\text{CoC} = \text{Effective orifice area} / \text{Geometric orifice area}. \quad (2)$$

LV Flow Energetics Across the Valve Models

We further postprocessed the LV velocity fields to extract fluid dynamics indices relevant to hemodynamics. Fundamental energetic properties of LV flow dynamics were characterized by several key parameters. For example, the normalized kinetic energy (KE) per unit volume is calculated as:

$$\text{KE}(t) = \frac{1}{V}\int_V \frac{1}{2}|\boldsymbol{u}|^2 dV; \quad (3)$$

where V is the 2-dimensional representation of whole LV volume, u is the velocity vector field. This metric quantifies the KE within the LV model's flow at each time point. Additionally, the rate of KE dissipation per unit volume (ε) is given by:

$$\varepsilon(t) = \frac{\nu}{V}\int_V \sum_{i,j}\left(\frac{\partial u_i}{\partial x_j}\frac{\partial u_i}{\partial x_j} + \frac{\partial u_i}{\partial x_j}\frac{\partial u_j}{\partial x_i}\right) dV; \quad (4)$$

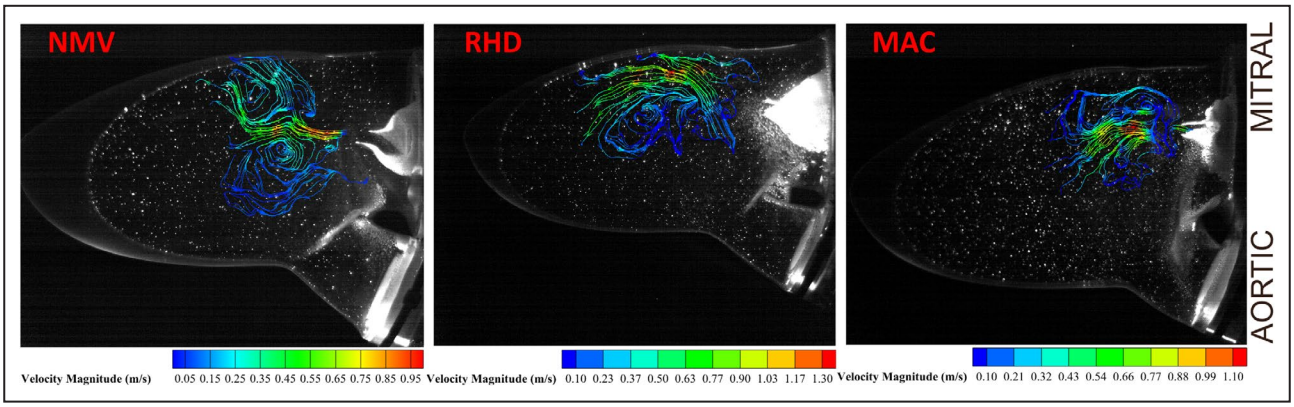

Figure 5. Transmitral flow visualization.
This image compares synchronized middiastolic transmitral flow, simulating (left) noncalcified healthy conditions (NMV), (middle) RMS, and (right) MAC in vitro. The streamlines shown represent the flow patterns within the laser-illuminated region, which corresponds to the laser sheet passing through the midplane of the valves. These streamlines are color coded on the basis of the magnitude of the flow velocity field. A consistent transmitral vortex ring was observed in NMV, whereas no visible vortex rings were detected in RMS and MAC. MAC indicates mitral annular calcification; NMV, normal mitral valve; and RMS, rheumatic mitral stenosis.

where x is the spatial location vector, i and j represent the spatial dimension indices, and ν is the kinematic viscosity. The rate of KE dissipation refers to the amount of KE that is converted into other forms of energy, such as heat, over time within a given system. In fluid dynamics, this concept is often used to describe how the motion of a fluid is gradually lost due to factors like friction, turbulence, and viscosity as it moves through a pipe, vessel, or heart valve.

RESULTS

Dimensional Variations Derived From 3-Dimensional Echocardiography

Table 2 displays data on diameters and areas at different points within the valve unit for the 3 different valve types. Figures 1 and 2 present the key measurements from the detailed data provided in Figures S1 and S2. Of note, the anteroposterior diameter of the MAC valve annulus was significantly smaller than that of RMS valve (P=0.003). Within the valve tunnel, the anteroposterior diameter in the MAC valve was again significantly smaller than in RMS valve (P<0.0001). At the leaflet tips, as expected, the anteroposterior diameter was smaller in both MAC and RMS valves compared with NMV, with no significant difference between RMS and MAC (P=0.156) (see Figure 6).

For the intercommissural diameter, there was no significant difference between MAC and RMS at the level of the annulus (P=0.126). Within the valve tunnel, intercommissural diameter was smaller in RMS and MAC compared with NMV, with no significant difference observed between RMS and MAC (P=0.096). At the leaflet tips, as expected, the intercommissural

Table 2. Comparative Measures in the Various Valve Types

		NMV	RMS	MAC	*P* value (RMS vs MAC)
Annulus	Anteroposterior diameter	3.36 (2.97–3.80)	3.55 (3.27–3.96)	3.16 (2.86–3.54)	0.003*
	Intercommissural diameter	4.12 (3.73–4.65)	4.18 (3.82–4.69)	3.89 (3.44–4.71)	0.126
	Area	10.96 (8.82–13.81)	11.36 (10.28–14.34)	10.01 (7.83–11.34)	0.021*
Tunnel	Anteroposterior diameter	2.54 (2.15–2.84)	2.27 (1.59–2.68)	1.38 (1.09–1.55)	<0.0001*
	Intercommissural diameter	2.84 (2.46–3.22)	2.27 (2.01–2.56)	2.04 (1.65–2.43)	0.096
	Area	5.51 (4.57–7.26)	4.23 (2.90–5.52)	2.92 (1.99–3.14)	0.002*
Leaflet tips	Anteroposterior diameter	2.05 (1.56–2.45)	0.89 (0.68–1.11)	1.00 (0.82–1.28)	0.156
	Intercommissural diameter	2.54 (2.33–2.72)	1.39 (1.09–1.62)	1.45 (1.08–2.01)	0.569
	Area	3.82 (2.40–5.20)	1.55 (0.85–2.25)	1.38 (1.13–2.16)	0.957
Tunnel length, cm		1.90 (1.67–2.09)	1.95 (1.81–2.11)	1.43 (1.31–1.81)	<0.0001*
MV volume, mL		19.8 (14.9–24.1)	20.1 (14.4–23.7)	7.0 (5.3–9.4)	<0.0001*

Measurements are presented as median (IQR).
IQR indicates interquartile range; MAC, mitral annular calcification; MV, mitral valve; NMV, normal mitral valve; and RMS, rheumatic mitral stenosis.
*Indicates statistical significance.

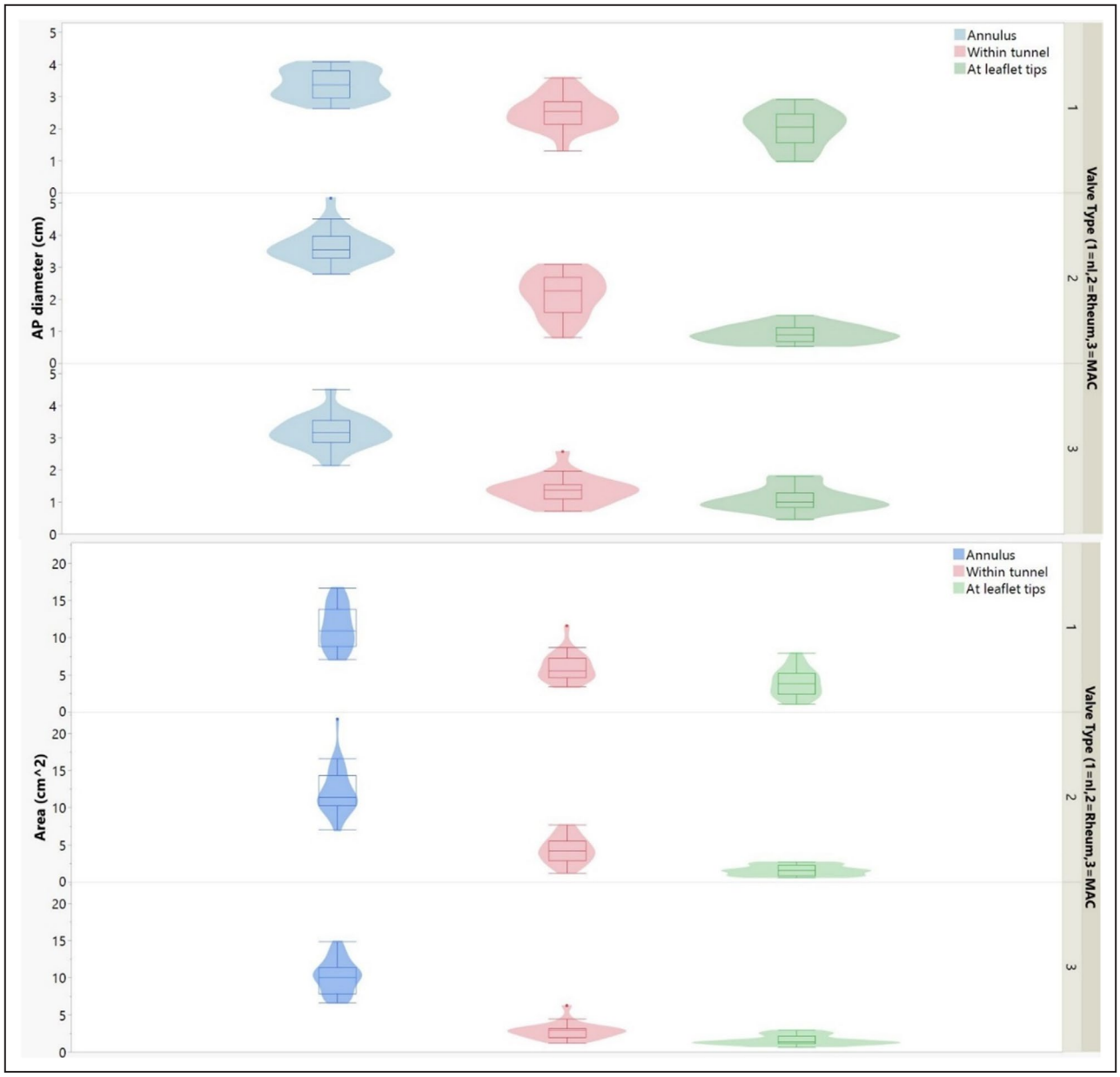

Figure 6. Dimensional variations at different levels within the mitral valve types.
The top panel displays box plots of anteroposterior diameter at different levels with the annulus/valve unit for each of the valve types. Note that the anteroposterior diameter diminishes gradually from annulus to leaflet tips in the NMV. In RMS, the anteroposterior diameter decreases markedly within the valve tunnel and is most decreased at the leaflet tips. In MAC MS, the anteroposterior diameter is a bit less at the annular level, dropping dramatically within the valve tunnel with little further decrease at the leaflet tips. The bottom panel displays box plots of the area for blood flow at the different levels within the annulus/valve unit for each of the valve types. Similar trends are seen. See also Table 2. AP indicates anteroposterior; MAC, mitral annular calcification; NMV, normal mitral valve; and RMS, rheumatic mitral stenosis.

diameter was smaller in MAC and RMS than in NMV, with no significant difference noted between RMS and MAC (P=0.569).

The annular area of the MAC valve was significantly smaller than that of the RMS valve (P=0.021). Within the valve tunnel, the area was significantly smaller in MAC compared with RMS (P=0.002). As expected, both MAC and RMS exhibited smaller areas at the leaflet tips compared with NMV, with no significant difference between the 2 (P=0.957) (see Figure 6).

The mitral tunnel length, measured from the midpoint of the annulus to the leaflet tips, was significantly shorter in MAC valves compared with RMS (P<0.0001). Likewise, the mitral valve volume was significantly smaller in MAC valves than in RMS (P<0.0001). This finding is notable, with the MAC valve appearing

Table 3. Comparing the Mitral Valve Orientations in NMV, RMS, and MAC

	Degrees from neutral (anteroposterior)	Posteriorly directed, %	Degrees from neutral (intercommissural)	Medially directed, %
NMV	4.0 (1.0–14.8)	77	1.5 (0.8–3.5)	64
RMS	19.2 (13.1–28.2)	85	6.3 (2.2–18.1)	35
MAC	14.3 (4.6–24.6)	55	7.9 (2.3–10.8)	59

Measurements are presented as median and interquartile range.
MAC indicates mitral annular calcification; NMV, normal mitral valve; and RMS, rheumatic mitral stenosis.

"shrunken" compared with RMS and NMV (Figure 3; Videos S1 through S3).

Power and effect size calculations were performed for some of the key anatomic variables (Table S1). These demonstrate ample power with our current sample size.

As summarized in Table 3, the orifice orientation relative to the annular plane shows minimal variation in NMV, as expected. In RMS valves, the median difference in the anteroposterior direction was 19°, with the orifice directed posteriorly in 85% of cases. In the intercommissural direction, the median difference was 6°, with a lateral orientation in 65% of cases. For MAC valves, the median difference in the anteroposterior direction was 14°, with the orifice oriented posteriorly in 55% of cases. In the intercommissural direction, the median difference was 8°, with the orifice directed medially in 60% of cases.

CoC Among the Pathological Models

The geometric orifice areas measured via 3-dimensional echocardiography were 1.4 cm^2 for the MAC model and 0.9 cm^2 for the RMS model. The effective orifice areas, estimated using PIV and flowmeter data, were 0.35, 0.45, and 0.56 cm^2 for the MAC, RMS, and NMV models, respectively. Consequently, the CoCs were calculated to be 0.35 for the MAC model and 0.50 for the RMS model.

The peak mitral jet velocities were 1.67, 1.3, and 1.05 m/s for MAC, RMS, and NMV models, respectively. The Reynolds number was calculated using the kinematic viscosity of water (1×10^{-6} m^2/s), the peak diastolic velocities, and the effective mitral orifice diameters, yielding values of 11 200, 9840, and 8866 for MAC, RMS, and NMV models, respectively. The Womersley numbers, based on the simulated heart rate of 70 bpm and the same characteristic diameters, were 9.05, 10.25, and 11.43 for MAC, RMS, and NMV models, respectively. These results are summarized in Table 4 and indicate turbulent flows at peak jet velocities in the in vitro experiments. More specifically, the Reynolds number of the MAC and RMS were significantly higher than the NMV. The Reynolds number we acquired for the NMV is in the range suggested by previous studies.[19–22] Higher magnitudes from the MAC and RMS models reflect stronger turbulence patterns, consistent with the observed flow behavior and associated energy loss.

Table 4. Comparing the Dimensionless Reynolds and Womersley Numbers Across the Valve Models Following Our In Vitro Experiments

	Reynolds number	Womersley number
NMV	8866	11.43
RMS	9840	10.25
MAC	11 200	9.05

MAC indicates mitral annular calcification; NMV, normal mitral valve; and RMS, rheumatic mitral stenosis.

To mimic the clinical approach for calculating pressure gradients, we applied the simplified Bernoulli equation to estimate pressure drops across the mitral valve:

$$\Delta P(\text{mm Hg}) = 4v(\text{m/s})^2.$$

The approximate maximum pressure drops observed in our experiments were 11.2 mm Hg for the MAC model, 6.8 mm Hg for the RMS model, and 4.4 mm Hg for the NMV model.

Comparison of Transmitral Flow In Vitro

A consistent transmitral vortex ring was observed in the NMV, while no visible vortex ring was detected in RMS and MAC valves (Figure 5; Videos S4 through S6). The data indicate that the transmitral jet begins to propagate earlier in the cardiac cycle and at higher velocities in the MAC valve compared with the other valves. Additionally, the transmitral velocities in RMS valve were higher than those of the NMV, but less than those of the MAC valve. However, the velocity toward the mitral valve during systole in the same region of interest was found to be similar across all conditions (Figure 7).

Comparison of LV Flow Energetics In Vitro

As shown in Figure 8, there are notable differences in the flow energetics profiles across the various mitral valve models. We found that MAC exhibited the highest-flow KE, while RMS flow KE was similar to that of NMV during diastole but lower during systole.

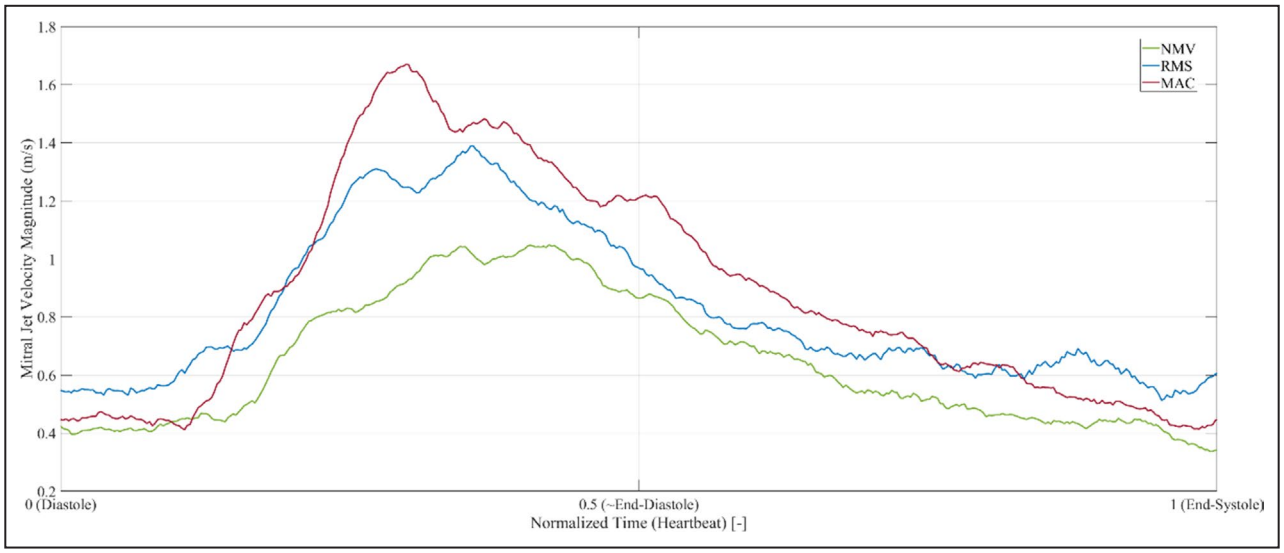

Figure 7. Comparison of transmitral flow velocity.
This figure compares the transmitral flow velocity profiles for NMV, RMS, and MAC during a representative cardiac cycle in vitro. The velocity profiles downstream of the mitral valve were calculated by averaging the velocity magnitudes within a region of interest parallel to the mitral valve annulus. The profiles are plotted using moving averages with a window of 10 data points to enhance the identification of differences and reduce noise. The horizontal axis represents normalized time, beginning at end-systole (ie, the beginning of diastolic filling). MAC indicates mitral annulus calcification; NMV, normal mitral valve; and RMS, rheumatic mitral stenosis.

Conversely, the rate of KE dissipation was highest in MAC during both phases. In diastole, however, the rate of dissipation in RMS was higher than in NMV, while during systole, this parameter was generally similar between RMS and NMV.

DISCUSSION

In this study, we compared MS caused by MAC with that caused by rheumatic disease, using the NMV as a reference. The study was conducted in 2 phases. First, we performed detailed measurements of each valve type using 3-dimensional TEE data sets from actual patients. Next, we selected a representative example of each valve type and used 3-dimensional printing to create silicone models for in vitro analysis. Using a heart flow simulator and laser PIV, we investigated how each valve type influenced formation of transmitral vortex ring and energy loss as distilled water flowed across the mitral valve and into the LV model. This approach allowed us to isolate the impact of valve morphology on these parameters, eliminating confounding influences from variable atrial and ventricular compliance.

The main findings of the clinical echocardiographic study are: (1) in MAC MS, both the annular area and the tunnel area are smaller than in rheumatic disease, primarily due to a greater reduction in the anteroposterior dimension; and (2) the volume enclosed by the annulus/valve unit is significantly smaller in MAC compared with RMS. As illustrated in Figure 6 (top panel) the anteroposterior diameter of the normal mitral valve gradually decreases from the annulus to the valve tunnel and toward the leaflet tips. In RMS, the anteroposterior diameter decreases markedly from the annulus to the valve tunnel and even further at the leaflet tips. In MAC MS, the anteroposterior diameter is already reduced at the annular level, becoming severely diminished in the valve tunnel with minimal further reduction at the leaflet tips. The blood flow area at different levels of the annulus/valve unit follows a pattern similar to that of the anteroposterior diameter (Figure 6, bottom panel). In RMS, the area progressively reduces, with the most severe stenosis occurring at the leaflet tips. By contrast, in MAC, severe stenosis occurs as soon as blood passes through the annulus and enters the calcium tunnel. This is in line with previous studies that have described the calcium tunnel as the source of functional stenosis.[6,23] Our findings expand on this concept, showing that a key feature of this MS phenotype is the marked reduction in anteroposterior dimension. As calcium extends from the annulus onto the leaflets, their bases become rigid, and their hinge points are displaced apically (Figure 9).[24] This leads to the characteristic shrunken valve seen in MAC-related MS (Figure 3). In contrast, rheumatic disease is marked by commissural fusion, producing a funnel-shaped stenosis and a larger annulus/valve unit volume.[25]

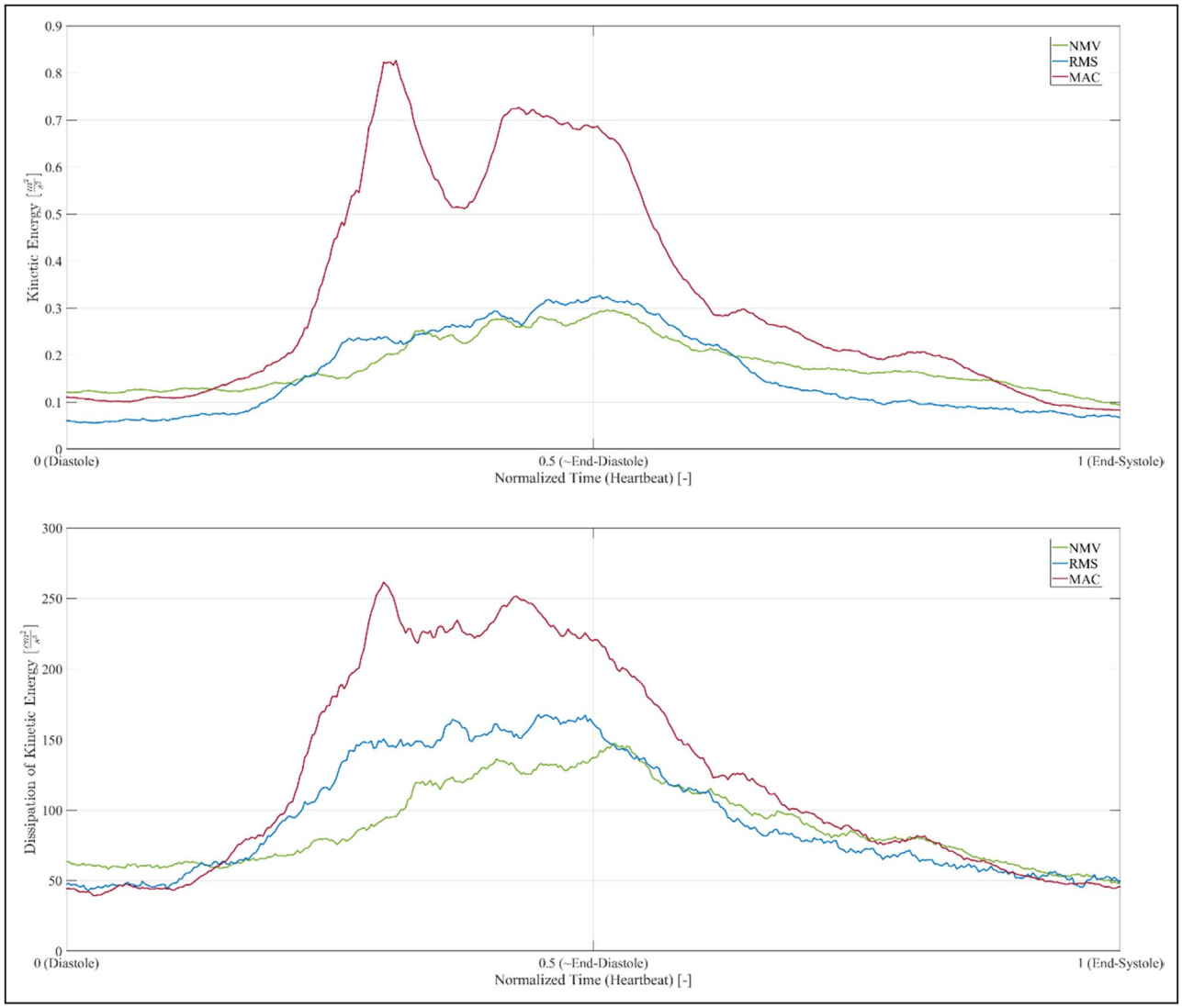

Figure 8. Comparison of left ventricular flow energetics in vitro.
This figure shows the time variations of 2 hemodynamic quantities—kinetic energy, *KE*(*t*), and dissipation rate, ε(*t*)—averaged over the left ventricular areas for a representative cardiac cycle in each in vitro experiment. To reduce noise and highlight differences, the data were plotted using moving averages with a window of 10 data points. The horizontal axis represents normalized time, starting at end-systole (ie, the beginning of diastolic filling). MAC indicates mitral annular calcification; NMV, normal mitral valve; and RMS, rheumatic mitral stenosis.

To better understand the effects of altered geometry on flow dynamics through the mitral valve, we conducted in vitro studies using 3-dimensional silicone models of each valve type. By using a heart flow simulator, we were able to control the heart rate and stroke volume flowing across the valve, removing the confounding effects of loading conditions and chamber compliances. Flow dynamics and transmitral vortex formation were studied using PIV. While a consistent transmitral vortex ring was observed in the normal mitral valve model, no visible vortex rings were found in the rheumatic or MAC models. Focusing on the MAC valve, higher-velocity early mitral inflow was observed compared with the rheumatic and NMV models. LV energetics analysis showed that the MAC valve exhibited the highest kinetic and dissipative energy profiles. This was true even though the geometric orifice area of the MAC valve model was greater than that of the RMS valve model. Two factors likely contributed to this difference: (1) The RMS valve has a larger volume and sloping leaflets, which causes less disruption to flow streams compared with MAC, where the small intravalvular volume and sudden obstruction from bulky calcific deposits at the leaflet bases greatly disrupt flow. (2) Due to the distinct valve morphology, MAC valves exhibit a smaller contraction coefficient than RMS valves, consistent with previous in vitro findings.[18] This leads to a smaller vena contracta when MAC is the cause

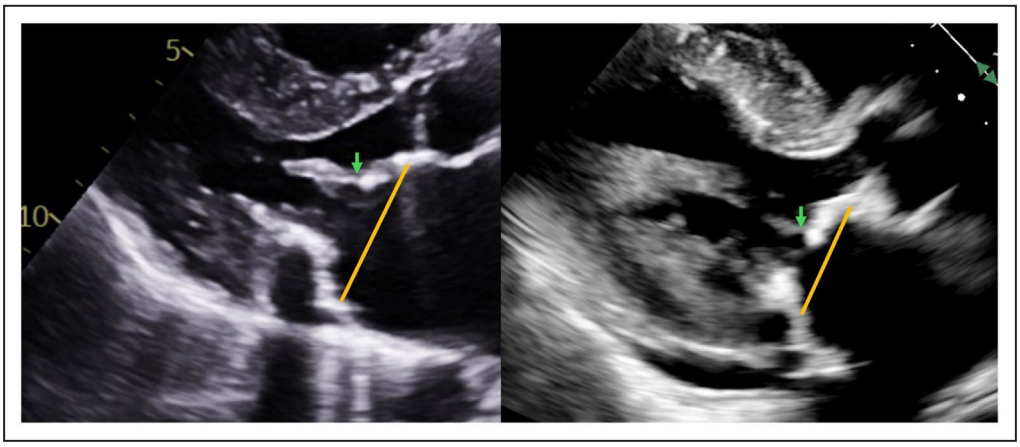

Figure 9. Apical displacement of the mitral valve leaflets in MAC.
The orange line indicates the position of the mitral annulus, and the short green arrow marks the hinge point of the anterior mitral leaflet. In a normal scenario, the hinge point is located at the leaflet's attachment to the annulus. However, in these 2 cases of severe MAC, the hinge point is displaced apically. Additionally, note the significantly reduced volume within the leaflet/annulus unit. MAC indicates mitral annular calcification.

of stenosis. Since the vena contracta determines the pressure drop across the valve, the MAC valve would be expected to produce a greater pressure drop than the RMS valve for the same geometric orifice area.

Severe MAC typically produces a transvalvular Doppler signal in vivo that is E-wave dominant, with a short deceleration time. In contrast, RMS often results in a Doppler signal where the E- and A-wave velocities are nearly equal, accompanied by a long deceleration time. (Figure 10). The differing Doppler profiles suggest that in severe MAC, flow across the mitral valve is primarily concentrated in early diastole, whereas in RMS, flow is more steady throughout diastole. This could potentially lead to differences in LV filling between the 2 disease states. MAC is typically associated with a small thick-walled ventricle[26,27] that relaxes slowly and would not well accommodate inflow of blood in early diastole. This leads to a rapid rise in LV diastolic pressure, further limiting transmitral flow and raising left atrial pressure. In rheumatic disease, unless there is significant ventricular pathology, the left ventricle fills more evenly through diastole, supported by the steady flow across the rheumatic valve. The findings in MAC are thought to result from the higher left atrial pressure

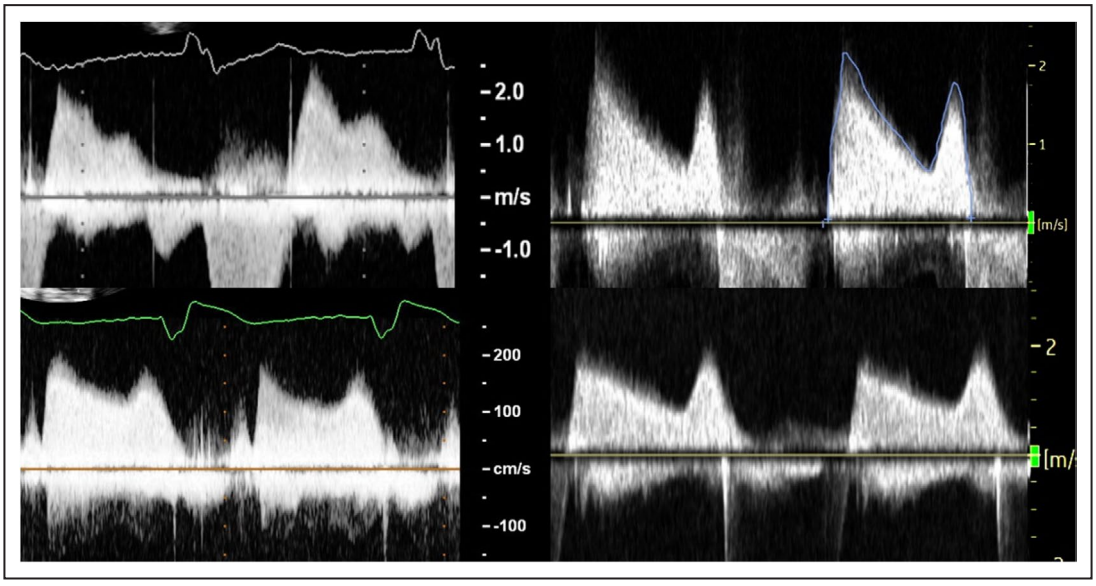

Figure 10. Comparison of continuous-wave Doppler signal in MAC versus RMS.
The top of the image shows 2 examples of the continuous-wave Doppler signal in MAC. Below, 2 examples of RMS are displayed. Note the steeper slope of the E-wave deceleration in MAC, compared with the longer deceleration time seen in RMS. MAC indicates mitral annular calcification and RMS, rheumatic mitral stenosis.

and reduced left atrial compliance typically seen in patients with MAC.[28] Yet in our in vitro study, where flow and chamber compliances were held constant, the MAC valve produced the highest E-wave velocity and earliest diastolic flow. Thus, it appears that the valve itself also contributes to the Doppler flow profile typically associated with MAC.

The higher energy losses associated with the MAC valve, coupled with its smaller contraction coefficient, result in a greater pressure drop across the MAC valve for a given geometric orifice compared with the RMS valve. We previously observed this in a study comparing echocardiograms of patients with MAC MS to those with RMS.[29] This makes interpreting the transvalvular pressure gradient and geometric orifice area challenging in patients with MAC, as the guidelines established for RMS cannot be applied. However, the existing literature indicate the prognostic significance of the transvalvular gradient in MAC MS.[30,31] As multiple factors influence the transvalvular gradient in patients with MAC, determining the severity of a patient's valve disease and whether intervention is necessary can be challenging. For now, we must rely on multimodal imaging (at rest and with exercise) in conjunction with clinical experience when making treatment decisions.

Study Limitations

One of the primary limitations of this study is the inherent restriction of 2-dimensional velocity measurement techniques, including our laser PIV method, in accurately capturing the full complexity of 3-dimensional flows, particularly in intricate geometries such as those found in the LV. Specifically, these techniques provide only the in-plane components of the 3-dimensional velocity vectors, which may lead to an incomplete characterization of flow dynamics.

There were a few practical constraints in our in vitro experiments. Distilled water was used instead of a blood analogue, and cardiac output was maintained at 3.5 L/min, below normal physiological levels. Two factors motivated the use of water: (1) *material compatibility*: glycerin solutions can swell and soften silicone valve models, altering mechanics and reproducibility; and (2) *optical clarity*: glycerin–water mixtures reduce transparency, limiting accuracy in PIV. In addition, the mitral valve's complex, saddle-shaped 3-dimensional geometry makes precise measurement of the CoC challenging, especially under pulsatile conditions. Our 3-dimensionally printed valve models enabled controlled geometry and standardized testing, with temporal and geometric dynamics captured by high-speed imaging at 1000 frames/s. To mitigate limitations, the same measurement approach was applied consistently across valve groups, allowing valid comparisons even if absolute CoC values cannot fully replicate physiological variability. The Reynolds number obtained for the NMV fell within the range of previously published data, indicating that the use of water as the working fluid, together with our valve dimensions and flow rate, produced comparable flow conditions.[19–22]

It is important to note that several studies have demonstrated that the simplified Bernoulli equation may either underestimate or overestimate pressure drops in different cardiac settings.[32–34] We fully agree with these previous findings and applied this approach here solely to maintain consistency with current clinical practice in Doppler echocardiography, which relies on the simplified Bernoulli equation.

Another limitation concerns the generalizability of our findings, as the sample size for the 3-dimensional echocardiographic morphological analysis was relatively small, limiting the strength of definitive conclusions. In this study, we aimed to establish feasibility and explore potential differences among NMV and RMS- and MAC-related MS using novel echocardiographic measurements. Despite the limited sample size, we observed consistent and statistically meaningful trends that highlight geometric differences among these groups. Patients with MAC MS and RMS were in advanced stages (C/D), and the available data do not allow conclusions regarding how geometric differences evolved or over what time frame. Consequently, the cohort did not allow robust stage-based stratification.

Finally, the experimental results are specific to the 3 valve prototypes representing NMV, RMS, and MAC. Although these 3-dimensional models reasonably approximate the respective disease states, they do not capture the full spectrum of anatomic and pathological variability seen in clinical practice. MAC exhibits considerable heterogeneity in severity and phenotypic presentation, and relying on a single representative geometry from each group inevitably limits generalizability. However, this approach allowed us to isolate and highlight the mechanistic effects of geometry and calcification on hemodynamics without confounding factors. While not fully generalizable, these findings provide foundational insights and establish a controlled comparison framework, demonstrating how variations in valve geometry and calcification can significantly influence LV hemodynamics and guiding future studies that incorporate a broader spectrum of MAC phenotypes.

Future studies should investigate a broader range of valve morphologies and pathophysiological conditions, particularly across the spectrum of MAC phenotypes and severities, to improve applicability to patient-specific scenarios. While the practical limitations of our in vitro setup did not affect comparative analyses among valve models, incorporating varying cardiac outputs and a more physiological blood analogue would yield additional clinically relevant insights.

CONCLUSIONS

This study highlights key morphological and hemodynamic differences between mitral stenosis caused by MAC versus rheumatic disease. Through a combination of clinical imaging and controlled in vitro modeling, we demonstrated that MAC-related stenosis is characterized by a smaller valve structure, greater energy loss, and altered flow dynamics that differ substantially from the rheumatic phenotype. These differences have important implications for diagnostic interpretation and treatment planning, underscoring the need for tailored assessment strategies, especially in patients with MAC for whom standard RMS guidelines do not apply.

ARTICLE INFORMATION

Received July 10, 2025; accepted December 2, 2025.

Affiliations

Department of Biomedical Engineering (M.S.H., A.K.) and Department of Radiological Sciences (A.K.), University of California Irvine, CA; Division of Cardiology, Jefferson Einstein Medical Center, Thomas Jefferson University, Philadelphia, PA (P.A., A.N., G.S.P.).

Acknowledgments

The authors appreciate and acknowledge the efforts of Nnaoma Agwu, Ashlin Diaz, and Taraz T. Toosky in designing, modifying, and manufacturing the new modular apparatus added to the KLAB heart flow simulator in preparation for the in vitro experimentations.

Sources of Funding

This study is supported by multiple grants from the National Heart, Lung, and Blood Institute (HL162687, HL153724, HL157631, and HL173809) and a grant from the National Science Foundation (Award No. 2109959).

Disclosures

There is no disclosure or conflict of interest.

Supplemental Material

Table S1
Figures S1-S2
Videos S1–S6

REFERENCES

1. Abramowitz Y, Jilaihawi H, Chakravarty T, Mack MJ, Makkar RR. Mitral annulus calcification. *J Am Coll Cardiol*. 2015;66:1934–1941. doi: 10.1016/j.jacc.2015.08.872
2. Kipourou K, O'Driscoll JM, Sharma R. Valvular heart disease in patients with chronic kidney disease. *Eur Cardiol Rev*. 2022;17:e02. doi: 10.15420/ecr.2021.25
3. El Sabbagh A, Parikh P, Ray J, Nishimura RA, Pislaru SV, Pellikka PA, Guerrero M, Hochwald A, Miranda WR. Mitral annulus calcium score in patients with calcific mitral stenosis undergoing invasive hemodynamic assessment. *J Am Heart Assoc*. 2024;13:e030540. doi: 10.1161/JAHA.123.030540
4. Wang TKM, Griffin BP, Xu B, Rodriguez LL, Popovic ZB, Gillinov MA, Pettersson GB, Desai MY. Relationships between mitral annular calcification and cardiovascular events: a meta-analysis. *Echocardiography*. 2020;37:1723–1731. doi: 10.1111/echo.14861
5. Oni E, Boakye E, Pressman GS, Dardari Z, Jha K, Szklo M, Budoff M, Nasir K, Hughes TM, Blaha MJ. The association of mitral annular calcification with cardiovascular and noncardiovascular outcomes: the multi-ethnic study of atherosclerosis. *Am J Cardiol*. 2024;225:75–83. doi: 10.1016/j.amjcard.2024.06.017
6. Churchill TW, Yucel E, Deferm S, Levine RA, Hung J, Bertrand PB. Mitral valve dysfunction in patients with annular calcification: JACC review topic of the week. *J Am Coll Cardiol*. 2022;80:739–751. doi: 10.1016/j.jacc.2022.05.032
7. Movva R, Murthy K, Romero-Corral A, Seetha Rammohan HR, Fumo P, Pressman GS. Calcification of the mitral valve and annulus: systematic evaluation of effects on valve anatomy and function. *J Am Soc Echocardiogr*. 2013;26:1135–1142. doi: 10.1016/j.echo.2013.06.014
8. Bhargav R, Pressman GS. *MAC attacks: unusual complications of mitral annular calcification*. 2025 Accessed January 27, 2025. https://www.acc.org/Latest-inCardiology/Articles/2024/04/16/11/02/MAC-Attacks.
9. Hatle L, Brubakk A, Tromsdal A, Angelsen B. Noninvasive assessment of pressure drop in mitral stenosis by Doppler ultrasound. *Heart*. 1978;40:131–140. doi: 10.1136/hrt.40.2.131
10. Falahatpisheh A, Kheradvar A. High-speed particle image velocimetry to assess cardiac fluid dynamics in vitro: from performance to validation. *Eur J Mech B Fluids*. 2012;35:2–8. doi: 10.1016/j.euromechflu.2012.01.019
11. Groves EM, Falahatpisheh A, Su JL, Kheradvar A. The effects of positioning of transcatheter aortic valves on fluid dynamics of the aortic root. *ASAIO J*. 2014;60:545–552. doi: 10.1097/mat.0000000000000107
12. Kheradvar A, Gharib M. On mitral valve dynamics and its connection to early diastolic flow. *Ann Biomed Eng*. 2009;37:1–13. doi: 10.1007/s10439-008-9588-7
13. Morisawa D, Falahatpisheh A, Avenatti E, Little SH, Kheradvar A. Intraventricular vortex interaction between transmitral flow and paravalvular leak. *Sci Rep*. 2018;8:15657. doi: 10.1038/s41598-018-33648-9
14. Stamhuis E, Thielicke W. PIVlab–towards user-friendly, affordable and accurate digital particle image velocimetry in MATLAB. *J Open Res Softw*. 2014;2:30.
15. Chu JW, Levine RA, Chua S, Poh KK, Morris E, Hua L, Ton-Nu TT, Hung J. Assessing mitral valve area and orifice geometry in calcific mitral stenosis: a new solution by real-time three-dimensional echocardiography. *J Am Soc Echocardiogr*. 2008;21:1006–1009. doi: 10.1016/j.echo.2008.05.010
16. Salustri A, Almaghrabi A. Mitral valve disease correlation between the most important echocardiographic parameters and haemodynamics. *EJ Cardiol Pract*. 2018;16:24.
17. Dean LS, Kern MJ. Measuring valve gradients and areas. *J Soc Cardiovasc Angiogr Interv*. 2022;1:100433. doi: 10.1016/j.jscai.2022.100433
18. Gilon D, Cape EG, Handschumacher MD, Jiang L, Sears C, Solheim J, Morris E, Strobel JT, Miller-Jones SM, Weyman AE, et al. Insights from three-dimensional echocardiographic laser stereolithography. *Circulation*. 1996;94:452–459. doi: 10.1161/01.CIR.94.3.452
19. Lin BA, Forouhar AS, Pahlevan NM, Anastassiou CA, Grayburn PA, Thomas JD, Gharib M. Color Doppler jet area overestimates regurgitant volume when multiple jets are present. *J Am Soc Echocardiogr*. 2010;23:993–1000. doi: 10.1016/j.echo.2010.06.011
20. Khalafvand SS, Hung T-K, Ng EY-K, Zhong L. Kinematic, dynamic, and energy characteristics of diastolic flow in the left ventricle. *Comput Math Methods Med*. 2015;2015:701945. doi: 10.1155/2015/701945
21. Govindarajan V, Mousel J, Udaykumar HS, Vigmostad SC, McPherson DD, Kim H, Chandran KB. Synergy between diastolic mitral valve function and left ventricular flow aids in valve closure and blood transport during systole. *Sci Rep*. 2018;8:6187. doi: 10.1038/s41598-018-24469-x
22. Kheradvar A, Gharib M. Influence of ventricular pressure drop on mitral annulus dynamics through the process of vortex ring formation. *Ann Biomed Eng*. 2007;35:2050–2064. doi: 10.1007/s10439-007-9382-y
23. Backhaus SJ, Uzun H, Rösel SF, Schulz A, Lange T, Crawley RJ, Evertz R, Hasenfuß G, Schuster A. Hemodynamic force assessment by cardiovascular magnetic resonance in HFpEF: a case-control substudy from the HFpEF stress trial. *EBioMedicine*. 2022;86:104334. doi: 10.1016/j.ebiom.2022.104334
24. Muddassir SM, Pressman GS. Mitral annular calcification as a cause of mitral valve gradients. *Int J Cardiol*. 2007;123:58–62. doi: 10.1016/j.ijcard.2006.11.142
25. Pandian NG, Kim JK, Arias-Godinez JA, Marx GR, Michelena HI, Chander Mohan J, Ogunyankin KO, Ronderos RE, Sade LE, Sadeghpour A, et al. Recommendations for the use of echocardiography in the evaluation of rheumatic heart disease: a report from the American Society of Echocardiography. *J Am Soc Echocardiogr*. 2023;36:3–28. doi: 10.1016/j.echo.2022.10.009

26. Movahed MR, Saito Y, Ahmadi-Kashani M, Ebrahimi R. Mitral annulus calcification is associated with valvular and cardiac structural abnormalities. *Cardiovasc Ultrasound*. 2007;5:14. doi: 10.1186/1476-7120-5-14
27. Eleid MF, Foley TA, Said SM, Pislaru SV, Rihal CS. Severe mitral annular calcification: multimodality imaging for therapeutic strategies and interventions. *JACC Cardiovasc Imaging*. 2016;9:1318–1337. doi: 10.1016/j.jcmg.2016.09.001
28. Reddy YNV, Murgo JP, Nishimura RA. Complexity of defining severe "stenosis" from mitral annular calcification. *Circulation*. 2019;140:523–525. doi: 10.1161/CIRCULATIONAHA.119.040095
29. Pressman GS, Ranjan R, Park DH, Shim CY, Hong GR. Degenerative mitral stenosis versus rheumatic mitral stenosis. *Am J Cardiol*. 2020;125:1536–1542. doi: 10.1016/j.amjcard.2020.02.020
30. Pasca I, Dang P, Tyagi G, Pai RG. Survival in patients with degenerative mitral stenosis: results from a large retrospective cohort study. *J Am Soc Echocardiogr*. 2016;29:461–469. doi: 10.1016/j.echo.2015.12.012
31. Bertrand PB, Churchill TW, Yucel E, Namasivayam M, Bernard S, Nagata Y, He W, Andrews CT, Picard MH, Weyman AE, et al. Prognostic importance of the transmitral pressure gradient in mitral annular calcification with associated mitral valve dysfunction. *Eur Heart J*. 2020;41:4321–4328. doi: 10.1093/eurheartj/ehaa819
32. Falahatpisheh A, Rickers C, Gabbert D, Heng EL, Stalder A, Kramer HH, Kilner PJ, Kheradvar A. Simplified Bernoulli's method significantly underestimates pulmonary transvalvular pressure drop. *J Magn Reson Imaging*. 2016;43:1313–1319. doi: 10.1002/jmri.25097
33. Menciotti G, Abbott JA, Aherne M, Lahmers SM, Borgarelli M. Accuracy of echocardiographically estimated pulmonary artery pressure in dogs with myxomatous mitral valve disease. *J Vet Cardiol*. 2021;35:90–100. doi: 10.1016/j.jvc.2021.03.003
34. Trzcinka A, Fox JA, Shook DC, Hilberath JN, Hartman G, Bollen B, Liu X, Worthington A, Shernan SK. Echocardiographic evaluation of mitral inflow hemodynamics after asymmetric double-orifice repair. *Anesth Analg*. 2014;119:1259–1266. doi: 10.1213/ane.0000000000000436